Results in Engineering 24 (2024) 103098

Contents lists available at ScienceDirect

Results in Engineering

journal homepage: www.sciencedirect.com/journal/results-in-engineering

Co-pyrolysis of plastic waste and macroalgae *Ulva lactuca*, a sustainable valorization approach towards the production of bio-oil and biochar

Obie Farobie [a,b,*], Apip Amrullah [c], Widya Fatriasari [d], Asep Bayu Dani Nandiyanto [e], Lusi Ernawati [f], Surachai Karnjanakom [g], Seng Hua Lee [h], Rangabhashiyam Selvasembian [i], Nur Izyan Wan Azelee [j], Muhammad Aziz [k]

[a] Department of Mechanical and Biosystem Engineering, IPB University, Indonesia
[b] Surfactant and Bioenergy Research Center (SBRC), IPB University, Indonesia
[c] Department of Mechanical Engineering, Lambung Mangkurat University, Indonesia
[d] Research Center for Biomass and Bioproducts, National Research and Innovation Agency (BRIN), Indonesia
[e] Universitas Pendidikan Indonesia, Indonesia
[f] Department of Chemical Engineering, Institut Teknologi Kalimantan, Indonesia
[g] Department of Chemistry, Rangsit University, Thailand
[h] Department of Wood Industry, Universiti Teknologi MARA (UiTM) Cawangan Pahang Kampus Jengka, Malaysia
[i] Department of Environmental Science and Engineering, SRM University-AP, India
[j] Faculty of Chemical and Energy Engineering, Universiti Teknologi Malaysia (UTM), Malaysia
[k] Institute of Industrial Science, University of Tokyo, Japan

ARTICLE INFO

Keywords:
Co-pyrolysis
Macroalgae
Plastic waste
Biochar
Marine pollution

ABSTRACT

To address the pressing demand for sustainable energy in light of environmental challenges, this study explored the synergetic effects of the co-pyrolysis of polyethylene terephthalate (PET) and *Ulva lactuca* macroalgae to yield bio-oil and biochar. The objective is to enhance the bio-oil quality for wider usability and to combat marine pollution. By employing co-pyrolysis, notable progress has been achieved in bio-oil yield and quality, particularly in hydrocarbon content, through the integration of PET. The highest bio-oil yield of 37.91 % was achieved under optimal conditions at 500 °C with a feedstock mixture consisting of 40 % *U. lactuca* and 60 % PET. Under these conditions, the bio-oil exhibited a significant increase in hydrocarbon content, reaching 57.16 %, which is essential for improving its energy potential. Biochar quality was also enhanced, with the biochar from a 70 % *U. lactuca* and 30 % PET blend showing a BET surface area of 20.18 m^2/g, compared to the initial 1.38 m^2/g of raw *U. lactuca*, indicating improved surface properties. This study presents a sustainable energy generation and environmental preservation approach, underscoring the potential of synergistically utilizing marine resources and plastic waste.

1. Introduction

The rising demand for fossil fuels due to the growing global population has worsened environmental issues such as the emission of greenhouse gases (GHGs). This situation necessitates innovative solutions to address fuel costs and environmental and health hazards. The search for sustainable, renewable energy sources has turned towards biofuels [1].

Research has focused on biomass for biofuel production via pyrolysis, highlighting the potential of first- and second-generation biomasses [2]. However, the use of first-generation feedstock can increase food prices owing to competition between food and fuel [3,4]. Second-generation biomass, while avoiding this issue, still requires significant resources such as freshwater and arable land. This has shifted the attention to third-generation biomass, particularly macroalgae, for biofuels. Compared with terrestrial plants, macroalgae such as *Ulva lactuca* (sea lettuce) grow rapidly, yield high amounts of biomass, and require shorter harvesting cycles [5]. *U. lactuca* grows widely in the intertidal marine environment worldwide, from temperate to tropical zones. It is edible and rich in nutrients, including vitamins, minerals, proteins, and dietary fibers. In addition, it is considered a potential biomass source because of its rapid growth rate and high biomass yield

* Corresponding author. Department of Mechanical and Biosystem Engineering, IPB University, IPB Darmaga Campus, Bogor, West Java, 16680, Indonesia.
E-mail address: obiefarobie@apps.ipb.ac.id (O. Farobie).

https://doi.org/10.1016/j.rineng.2024.103098
Received 23 July 2024; Received in revised form 26 September 2024; Accepted 8 October 2024
Available online 11 October 2024

[6].

Algae can be classified into two main categories: microalgae and macroalgae. Microalgae are single-celled organisms that range in size from less than 2 μm to a few centimeters. In contrast, macroalgae are multicellular and can grow into large, visible structures, with some species reaching lengths of up to 60 m [7]. Both microalgae and macroalgae have been studied as potential feedstocks for biofuel production, but there are distinct advantages to using macroalgae. Macroalgae typically grow faster, can be harvested in larger quantities, and do not require specialized cultivation facilities as microalgae often do. Furthermore, microalgae cultivation generally involves higher costs and complex processing techniques to achieve meaningful biofuel yields, which can limit their large-scale feasibility [8]. In contrast, macroalgae, particularly *U. lactuca*, is more readily available, easier to harvest, and can be grown without competing for arable land, making it an economically and environmentally attractive choice for biofuel production [9].

Technologies such as gasification, pyrolysis, and hydrothermal liquefaction have been explored to transform biomass and waste into biofuels. Pyrolysis is particularly effective and adaptable to various feedstocks [10]. Gasification, while capable of producing syngas, operates at much higher temperatures (typically above 700 °C), making it more energy-intensive and costly compared to pyrolysis. Gasification often requires extensive pre-treatment of feedstocks and produces lower bio-oil yields [11]. On the other hand, hydrothermal processing involves the conversion of biomass in a water-based environment under high pressure, which can handle wet feedstocks without the need for drying. However, it generally results in lower bio-oil yields and is less efficient for large-scale applications [12]. These drawbacks make pyrolysis more favorable for this research, as it operates at moderate temperatures, can process a wide variety of feedstocks, and yields higher bio-oil output.

Previous studies have confirmed the viability of macroalgae in pyrolysis, noting benefits such as lower phenolic compound content, which simplifies oil upgrading [13]. However, the high oxygen content in macroalgae-derived oils lowers their heating value and requires extensive refining [14]. Co-pyrolyzing macroalgae with hydrogen-rich waste, such as plastics, which are mainly composed of carbon and hydrogen, can enhance oil quality by contributing to hydrogen during pyrolysis [15]. During the co-pyrolysis of biomass and hydrogen-rich plastics, the decomposition of plastics, primarily composed of carbon and hydrogen, releases a significant amount of hydrogen gas. Hydrogen can react with the intermediate products of biomass pyrolysis, facilitating the formation of hydrocarbons and reducing the production of oxygenated and nitrogenated compounds. The presence of hydrogen in the reaction environment helps saturate carbon radicals and stabilize the molecular structure of the resulting bio-oil, leading to an increase in the yield of hydrocarbons [16].

Several studies have demonstrated that co-pyrolysis, involving the simultaneous pyrolysis of biomass and plastic, can enhance the quality of the resultant bio-oil compared to pyrolysis of either component alone. For instance, Yang et al. [17] found that the co-pyrolysis of biomass residues with low-density polyethylene (LDPE) produced a bio-oil with a higher hydrocarbon content and reduced oxygenated compounds, leading to an overall improvement in oil quality. Similarly, the research by Cao et al. [18] observed that the co-pyrolysis of macroalgae and PVC led to a bio-oil with increased aromatic and aliphatic hydrocarbon yields, which are desirable components for high-quality fuel. Lee and colleagues [19] demonstrated that co-pyrolysis of polypropylene and brown algae with catalytic Al-SBA-15 reduced water content in bio-oil, increasing its quality. Kositkanawuth et al. [10] and Abomohra et al. [11] found that integrating polystyrene with macroalgae in pyrolysis improved the oil yield and quality and reduced biochar formation.

Despite these advances, there is still a substantial lack of detailed research on the co-pyrolysis involving *U. lactuca* and polyethylene terephthalate (PET). The novelty of this study lies in its first comprehensive examination of the co-pyrolysis of *U. lactuca* and PET. Thus, this research aimed to investigate this combination for renewable energy production from waste, specifically focusing on comparing the quality and quantity of oil at different mixture ratios and examining the characteristics of solid products from co-pyrolysis, which can be utilized as either a solid fuel or a soil amendment. This study aims to contribute to both sustainable energy advancement and marine pollution mitigation by valorizing marine and plastic wastes.

2. Experimental studies

2.1. Biomass preparation and characterization

U. lactuca (ULV) was sourced from Lombok Island in Indonesia. The algae were washed to remove debris, air-dried, and oven-dried for 12 h at 110 °C. The algae were ground using an electrical grinder (Willman, DE-100g). The sample was then sieved to achieve a uniform size of 0.25 mm using a test sieve (Nexopart, Germany). The PET flakes were obtained from PT. Pradha Karya Perkasa, Indonesia. The PET material was then ground and sieved to 0.5 mm. Five blends of algae and PET (70ULV:30PET, 60ULV:40PET, 50ULV:50PET, 40ULV:60PET, and 30ULV:70PET) were prepared. To prepare the different compositions, 50 g of *U. lactuca* was used for the 100ULV sample. For the other mixtures: 35 g of *U. lactuca* was combined with 15 g of PET for the 70ULV:30PET sample, 30 g of *U. lactuca* with 20 g of PET for the 60ULV:40PET sample, 25 g of *U. lactuca* with 25 g of PET for the 50ULV:50PET sample, 20 g of *U. lactuca* with 30 g of PET for the 40ULV:60PET sample, and 15 g of *U. lactuca* with 35 g of PET for the 30ULV:70PET sample.

The proximate analysis of the sample was conducted using a thermogravimetric analyzer (TGA 4000, PerkinElmer, USA) according to ASTM E1131-08 standards. The moisture content (MC) was measured based on the mass loss after the sample was heated to 110 °C in an N_2 atmosphere. The volatile matter (VM) was quantified by observing the mass loss at 900 °C. Subsequently, N_2 was replaced with air, and the ash content (AC) was determined by maintaining the sample isothermally at 900 °C for 45 min. The following equation was employed to deduce FC:

$$\text{FC (wt\%)} = 100 - (\text{AC wt\%} + \text{MC wt\%} + \text{VM wt\%}) \quad (1)$$

where, AC signifies ash content, MC denotes moisture content, VM represents volatile matter, and FC stands for fixed carbon.

Higher heating values (HHVs) were determined with a Parr 6200 bomb calorimeter (ASTM D 5865-04), and elemental analyses were performed using Leco CHN628 analyzer. The analytical results were verified in triplicate. The HHV of the pyrolysis products was calculated using a correlation equation based on prior research [20].

$$\text{HHV (MJ/kg)} = -1.3675 + (0.3137\text{C}) + (0.7009\text{H}) + (0.0318\text{O}) \quad (2)$$

Meanwhile, the lower heating value (LHV) was derived from the HHV using Eq. (3), as shown below:

$$\text{HHV (MJ/kg)} = \text{HHV} - [2.442 \times 8.936(\text{H}/100)] \quad (3)$$

2.2. Pyrolysis of U. lactuca and PET

The experiment was performed in a batch vessel equipped with a condenser and a thermocouple (Fig. 1). The reactor used in this experiment is a cylindrical vessel with a height of 0.50 m. The reactor has an inner diameter (ID) of 0.035 m and an outer diameter (OD) of 0.05 m and is constructed from stainless steel grade SS 316. The reactor is housed within an electric furnace, which ensures uniform thermal distribution across its surface during the experimental procedure. The vessel was loaded with 50 g of desiccated raw material, purged with nitrogen, and heated from normal temperature to 400–600 °C at 20 °C/min.

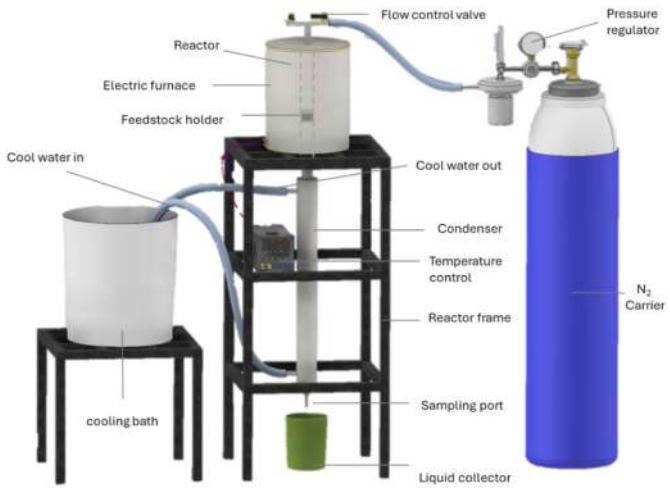

Fig. 1. Schematic of the pyrolysis reactor.

After reaching these temperatures, the vapor was collected via a liquid sample port. Water was extracted from the solution using anhydrous sodium sulfate. Vacuum filtration was used to separate the liquid. Gravimetric techniques were used to determine bio-oil and biochar yields, and the experiments were repeated three times for accuracy. The product yield calculations were calculated as follows.

$$Y_{bio-oil} = \frac{m_{bio-oil}}{m_{feedstock}} x\,100\% \quad (4)$$

$$Y_{biochar} = \frac{m_{biochar}}{m_{feedstock}} x\,100\% \quad (5)$$

$$Y_{gas} = 100\% - (Y_{bio-oil} + Y_{biochar}) \quad (6)$$

where $Y_{bio\text{-}oil}$, $Y_{biochar}$, and Y_{gas} refer to the yields of bio-oil, biochar, and gases, respectively; $m_{bio\text{-}oil}$ and $m_{biochar}$ signify their respective masses; and $m_{feedstock}$ represents the initial feedstock mass.

2.3. Bio-oil and biochar analyses

The bio-oil was analyzed using gas chromatography/mass spectrometry (GC/MS) with an Rtx-5MS column. The specific temperatures and detailed analysis have been described in our previous paper [14]. For biochar, a Hitachi SU 3500 scanning electron microscope (SEM) was used to analyze the surface morphology. In addition, morphological characterization was performed using a Talos F200C G2 High-Resolution Transmission Electron Microscope (HRTEM) operated at 200 kV. The sample was deposited onto a TEM grid and subsequently observed using the Talos F200C G2 (S)TEM system. At the same time, Brunauer-Emmett-Teller (BET) analysis was employed to examine the porosity and surface area using a Quantachrome Nova series analyzer, degassing biochar at 120 °C for 3 h. Similar to the feedstock analysis, the elemental composition of the biochar (C, H, N, S, and O) was determined using a CHN628 elemental analyzer (Leco, United States).

3. Results and discussion

3.1. Characterization of feedstock

Significant differences were observed in the proximate and ultimate analyses of the feedstock characteristics of *U. lactuca* and PET. These differences offer valuable insights into the potential and behavior of these materials during pyrolysis. The proximate and elemental compositions of each feedstock used in this study are listed in Table 1. Upon analyzing the composition, it was found that *U. lactuca* has a significantly higher ash content (42.1 %) compared to PET (0.8 %). The elevated ash content observed in marine macroalgae is a common characteristic, and it consists of minerals and trace elements that are responsible for the increased residue following pyrolysis [21]. The volatile matter content of *U. lactuca* was 49.7 %, which was lower than that of PET (82.1 %). This indicates that a larger fraction of *U. lactuca* is nonvolatile (bound as ash or fixed carbon).

The ultimate analysis highlighted that *U. lactuca* and PET differ significantly in their elemental compositions. *U. lactuca* contains 39.1 % carbon, 6.2 % hydrogen, 4.5 % nitrogen, 7.3 % sulfur, and 42.9 % oxygen. The combination of high oxygen content and low carbon content led to a high oxygen-to-carbon (O/C ratio). A high oxygen-to-carbon (O/C) ratio is unfavorable for fuel applications because it results in a lower heating value due to the significant amount of oxygen present. A significant quantity of sulfur is obtained from sulfate polysaccharides that are abundantly found in marine algae [22].

In contrast, PET demonstrated a lower oxygen content (32.2 %) and higher carbon content (63.4 %), as well as negligible nitrogen (0.1 %) and no sulfur. This elemental composition corresponds to a higher heating value because a higher carbon content implies that more energy can be released during combustion. Similar compositions have been noted in other studies, reinforcing the high energy potential of PET [23].

3.2. Product yields

An investigation into the behavior of *U. lactuca* and PET during pyrolysis at different temperatures and feedstock ratios yielded valuable insights into the production of bio-oil, biochar, and gas products. Fig. 2 shows the yields of co-pyrolysis products at various *U. lactuca* to PET ratios and temperatures of 400, 500, and 600 °C. When using pure *U. lactuca*, the production of biochar was significantly high at all of the temperatures that were tested. At a temperature of 400 °C, the yield was 82.31 %. However, as the temperature increased, the yield decreased (70.29 % at 500 °C and 66.49 % at 600 °C). Nevertheless, the yield remained considerably higher than that of mixtures containing PET. This higher solid residue is in line with the studies by Ross et al. [13], who suggested that the inherent trace elements and minerals found in macroalgae contribute to an increase in ash content, resulting in increased biochar yields.

The incorporation of PET into the feedstock blend systematically decreased the production of biochar, while simultaneously increasing the production of bio-oil at all temperature ranges investigated. For instance, at 400 °C, the biochar yield decreased from 82.31 % (pure *U. lactuca*) to 32.78 % when the feedstock contained 70 % PET. Conversely, the yield of bio-oil increased from 12.49 % to 27.11 % over the same feedstock composition range. This inverse relationship is likely because of the absence of ash in PET and the catalytic influence of

Table 1
Chemical and elemental analysis of the raw material.

No	Feedstock	Chemical Analysis (wt%)				Elemental Analysis (wt%)					HHV (MJ/kg)
		MC	VM	FC	AC	C	H	N	S	O	
1	*U. lactuca*	7.2	49.7	1.0	42.1	39.1	6.2	4.5	7.3	42.9	12.04
2	PET	0.4	82.1	16.7	0.8	63.4	4.3	0.1	0.0	32.2	45.81

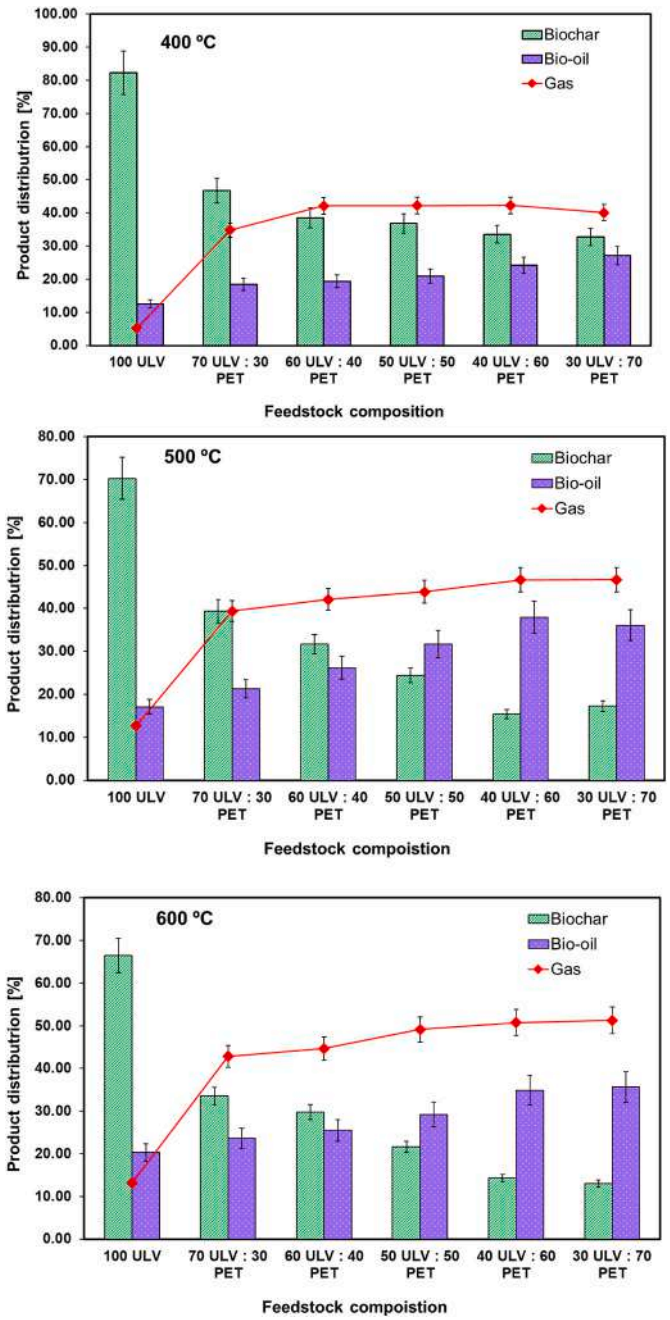

Fig. 2. Percent co-pyrolysis of the products of *U. lactuca* and PET at various temperatures.

minerals from *U. lactuca* on volatile formation, particularly at higher temperatures, such as 600 °C [24,25]. Moreover, the hydrogen radicals produced during PET pyrolysis are instrumental in promoting the breakdown of polymeric groups within biomass, thereby enhancing bio-oil formation [26].

The highest yield of bio-oil (37.91 %) was found at 500 °C with a feedstock ratio of 40 % *U. lactuca* to 60 % PET. This optimal temperature and composition combination suggests that moderate temperatures favor the synergetic effects of the components, resulting in maximum liquid product yields. Nevertheless, with the rise in temperature from 500 to 600 °C, there was a marginal decrease in the production of bio-oil, resulting in a yield of 35.64 % for the same feedstock ratio. This reduction can be attributed to additional cracking processes at higher temperatures, which lead to increased production of non-condensable gases [24]. The elevated gas yields at 600 °C confirm the enhanced cracking activity. Moreover, the decrease in the yield of biochar as temperature and PET content increase aligns with findings by Selvarajoo et al. [27], who observed a significant drop in pyrolysis char yields from 54.83 wt% to 26.67 wt% as temperatures increased from 300 °C to 900 °C.

3.3. Bio-oil composition

The bio-oil composition derived from the co-pyrolysis of PET and *U. lactuca* displays notable variations in composition depending on the temperature and feedstock ratio. The GC-MS analysis, as illustrated in Fig. 3, reveals significant differences in the chemical composition of bio-oils derived from the pyrolysis of *U. lactuca* alone compared to a co-pyrolysis blend of *U. lactuca* and PET. When *U. lactuca* was pyrolyzed independently, the bio-oil primarily consisted of compounds such as phenolics, N-aromatic compounds, amines/amides, and carboxylic acids. These compounds are characteristic of macroalgae pyrolysis [28]. However, when PET was introduced into the pyrolysis process, the chemical profile of the resulting bio-oil changed notably. The presence of PET led to the formation of new aromatic hydrocarbons, such as p-xylene, naphthalene, and anthracene, which are typically associated with the degradation of PET. This shift in chemical composition suggests that co-pyrolysis with PET not only enhances the diversity of compounds in the bio-oil but also introduces valuable aromatic hydrocarbons.

The distribution of bio-oil compositions derived from the co-pyrolysis of ULV: PET at different temperatures is presented in Fig. 4. Pure *U. lactuca* pyrolysis predominantly yielded bio-oils rich in carboxylic acids (22.63 %), phenolics (31.89 %), and amines/amides (15.33 %). These components are typically associated with the thermal degradation of marine biomass. Carboxylic acids derived from lipid decomposition are consistent with prior results obtained by Iaccarino et al. [28], showing similar patterns in other marine biomasses. Phenolics are likely to emerge from the degradation of nitrogenous components such as amines/amides and N-aromatic compounds and the steam reforming of aromatic substances, hinting at protein breakdown during pyrolysis [22,29]. A possible series of reaction mechanisms for the co-pyrolysis of *U. lactuca* and PET is illustrated in Fig. 5.

At 400 °C, there was a noticeable increase in hydrocarbon content with the rise in the ratio of PET in the blend, reaching up to 53.32 % at a blend ratio of 30 % *U. lactuca* and 70 % PET. Concurrently, the concentrations of phenolics, N-aromatics, amines/amides, carboxylic acids, ketones, and furan derivatives declined substantially. This suppression of undesired compounds suggests that co-pyrolysis with PET effectively modifies the product distribution by inhibiting the formation of certain organic compounds, thus potentially improving bio-oil quality.

Raising the pyrolysis temperature to 500 °C significantly altered the composition of bio-oil. For pure *U. lactuca*, considerable amounts of carboxylic acids (28.02 %), amines/amides (23.31 %), and phenolics (20.16 %) remained. However, the inclusion of PET resulted in a notable increase in hydrocarbon content, peaking at 57.16 % for the highest PET blend (30 % *U. lactuca* and 70 % PET). The constant levels of carboxylic acids at higher PET contents could result from secondary reactions promoted by the oligomerization of PET, which impacts the overall reaction pathway during condensation [24]. The enrichment of hydrocarbons at this temperature was accompanied by significant reductions in phenolics, N-aromatics, and amines/amides, echoing similar trends observed at 400 °C.

At 600 °C, the bio-oil composition shifts further towards hydrocarbons, which dominate the bio-oil composition at this elevated temperature. The highest hydrocarbon content of 63.62 % was achieved at a blend ratio of 30 % *U. lactuca* and 70 % PET. This temperature allows for greater thermal and secondary cracking, enhancing the formation of volatile hydrocarbon fractions while further reducing the presence of phenolics, carboxylic acids, amines/amides, N-aromatics, and minor components, such as ketones and furan derivatives. The persistent increase in hydrocarbons with increasing temperature and PET proportion

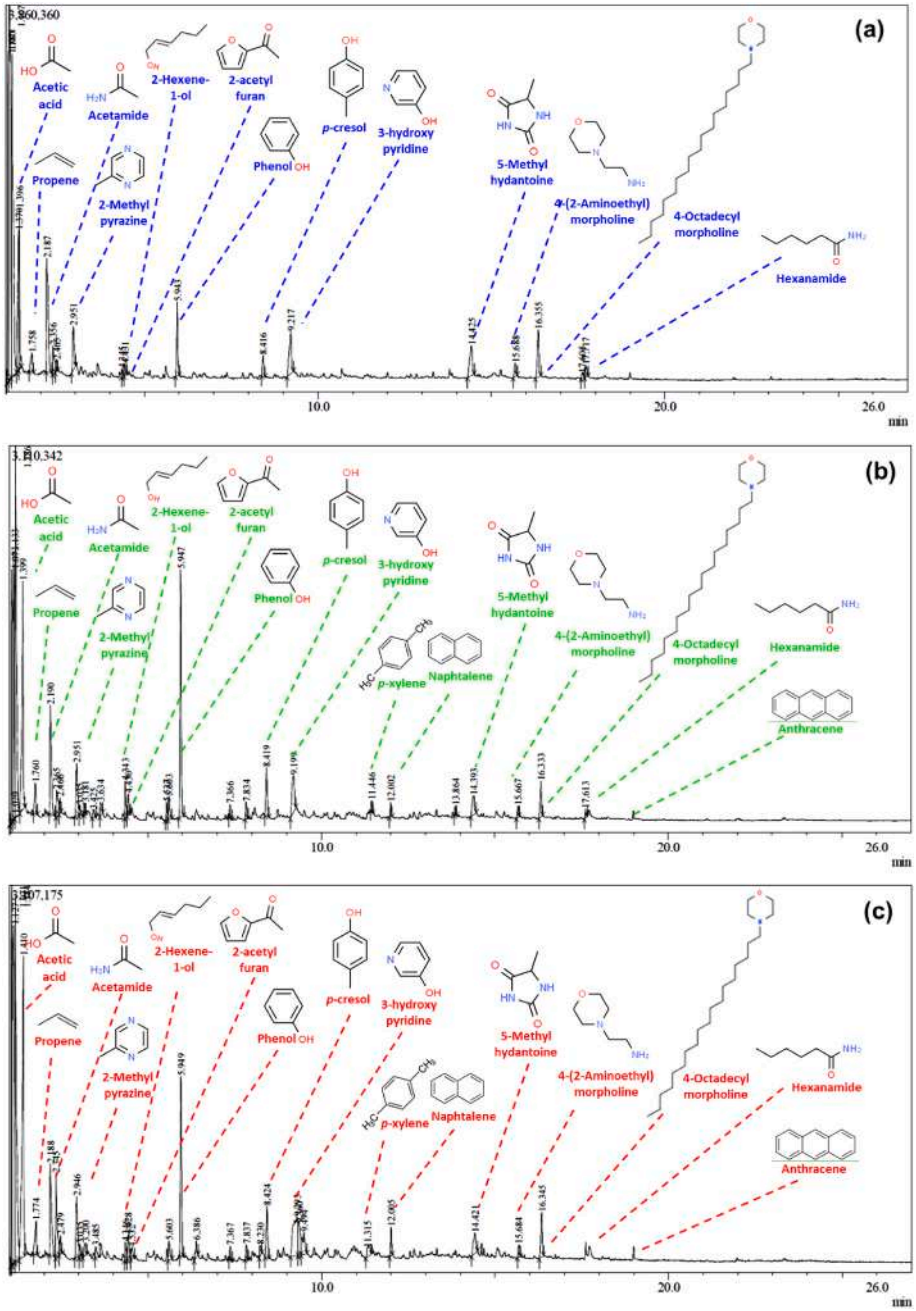

Fig. 3. GC–MS analysis of bio-oils obtained from pyrolysis of (a) individual *U. lactuca*, (b) 70 ULV: 30 PET, and (c) 30 ULV: 70 PET at 500 °C.

verified the cooperative impact of *U. lactuca* and PET in co-pyrolysis. This synergy amplifies bio-oil quantity, enhances its chemical composition to boost energy-rich hydrocarbons, and minimizes problematic oxygenated and nitrogenous elements.

3.4. Biochar characterization

The biochar resulting from the co-pyrolysis of *U. lactuca* and PET was analyzed using SEM to investigate any morphological changes that occurred after pyrolysis. The scanning electron microscopy (SEM) images presented in Fig. 6 provide essential information regarding the surface and structural changes of *U. lactuca* and its corresponding biochar at various feedstock ratios, specifically at a pyrolysis temperature of 500 °C. The SEM images revealed significant differences in the surface morphology between the untreated *U. lactuca* feedstock and the biochar produced from different feedstock ratios. The original *U. lactuca* feedstock exhibited the largest physical size, with a relatively smooth surface. However, after pyrolysis, the biochar surface deformed, displaying numerous cracks and voids. This deformation is primarily caused by the rapid volatilization of organic compounds, which results in the formation of a porous structure [28].

Increasing the PET content to 60 % and 70 % resulted in biochar with progressively larger physical sizes, showing significant compaction and agglomeration compared with biochar with lower PET content. This agglomeration is likely due to the sintering effects of the plastic polymer, which can cause biochar particles to adhere more closely, thereby reducing their overall porosity [30].

The HRTEM images in Fig. 7 provide a detailed examination of the structural properties of *U. lactuca* and biochar produced from various mixtures of *U. lactuca* and PET during co-pyrolysis. The raw *U. lactuca* (Fig. 7a) shows a smooth surface with no discernible graphitic structures or pores, which is characteristic of raw organic material prior to thermal

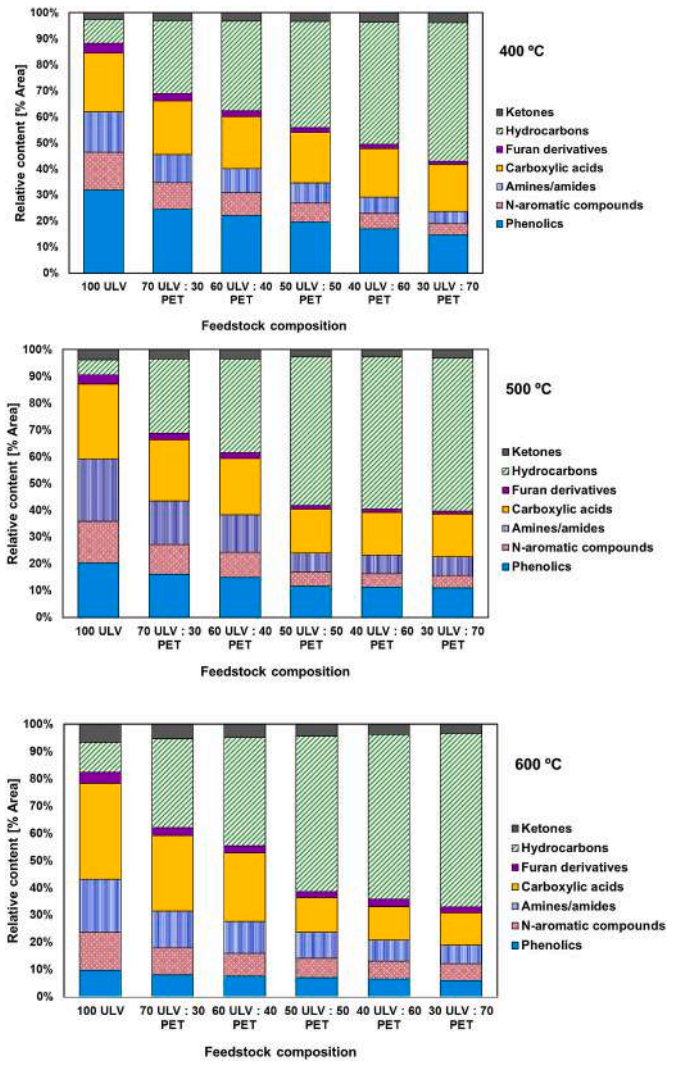

Fig. 4. Distribution of bio-oil compositions derived from the co-pyrolysis of ULV:PET at different temperatures.

treatment. However, in Fig. 7b, representing the biochar derived from a mixture of 70 % ULV and 30 % PET, the formation of graphitic carbon layers and irregular surface structures become evident. In Fig. 7c, with a mixture of 60 % ULV and 40 % PET, the graphitic carbon layers become more evident, and a more irregular surface structure starts to emerge. The biochar with 50 % PET (Figs. 7d) and 60 % PET (Fig. 7e) shows enhanced lamellar structures and the presence of fine pores, indicating increased graphitization and carbon reorganization. At 70 % PET (Fig. 7f), the biochar demonstrates well-developed graphitic layers, reflecting significant improvement in the carbon structure.

The BET analysis provided in Fig. 8 highlights the surface properties and pore structures of biochar produced from different compositions of *U. lactuca* and PET. The isotherms observed resemble the standard type IV isotherm pattern, indicating a significant presence of mesoporous structures in the biochar [31]. Table 2 compares the BET surface area to demonstrate how altering the feedstock ratios impacts the morphological characteristics of the biochar produced. The BET surface area of the raw *U. lactuca* feedstock is initially quite low, at 1.38 m^2 g^{-1}, with a mean pore diameter of 1.54 nm. However, upon pyrolysis and co-pyrolysis with PET, there was a marked increase in the mean pore diameter and BET surface area of biochar. For instance, biochar produced from a 70 % *U. lactuca* and 30 % PET blend exhibited a significantly enhanced BET surface area of 20.18 m^2 g^{-1} and a mean pore diameter of 12.41 nm. This substantial growth in the surface area and pore size may be attributed to the volatilization of organic materials at high temperatures, generating a porous and highly developed surface structure [28].

However, increasing the PET ratio in the feedstock composition leads to a consistent decline in the mean pore diameter and BET surface area of the biochar. For example, with a 60 % *U. lactuca* and 40 % PET blend, the BET surface area decreases to 18.56 m^2 g^{-1}, and the mean pore diameter decreases to 11.47 nm. This downward trend continued with increasing PET proportion, dropping to a BET surface area of 10.64 m^2 g^{-1} and a mean pore diameter of 6.48 nm when the biochar consisted of 30 % *U. lactuca* and 70 % PET. The reduction in the BET surface area and mean pore diameter with increasing PET content might be due to the agglomeration of the plastic polymer during pyrolysis [30]. Sintering can cause surface structures to coalesce, reducing the overall porosity and surface area of the biochar. The plastic material may partially melt and flow, potentially closing off some of the biochar's pore structures and leading to a more compact and less porous material.

The results presented in Table 3 highlight the elemental analysis of biochar derived from the co-pyrolysis of *U. lactuca* and PET. A key

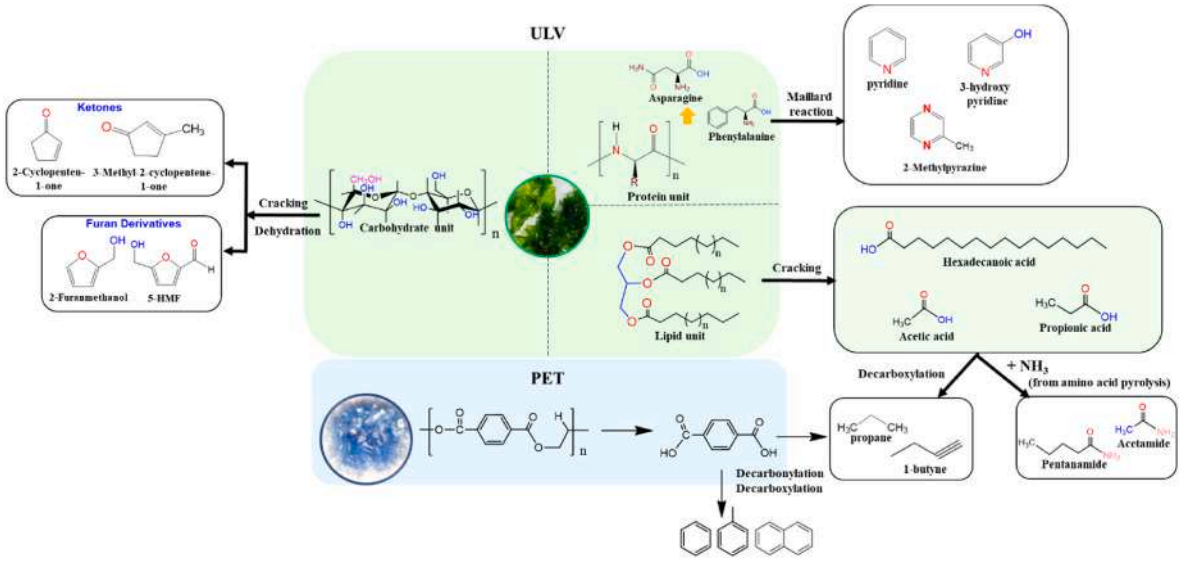

Fig. 5. A plausible reaction mechanism for the co-pyrolysis of *U. lactuca* and PET.

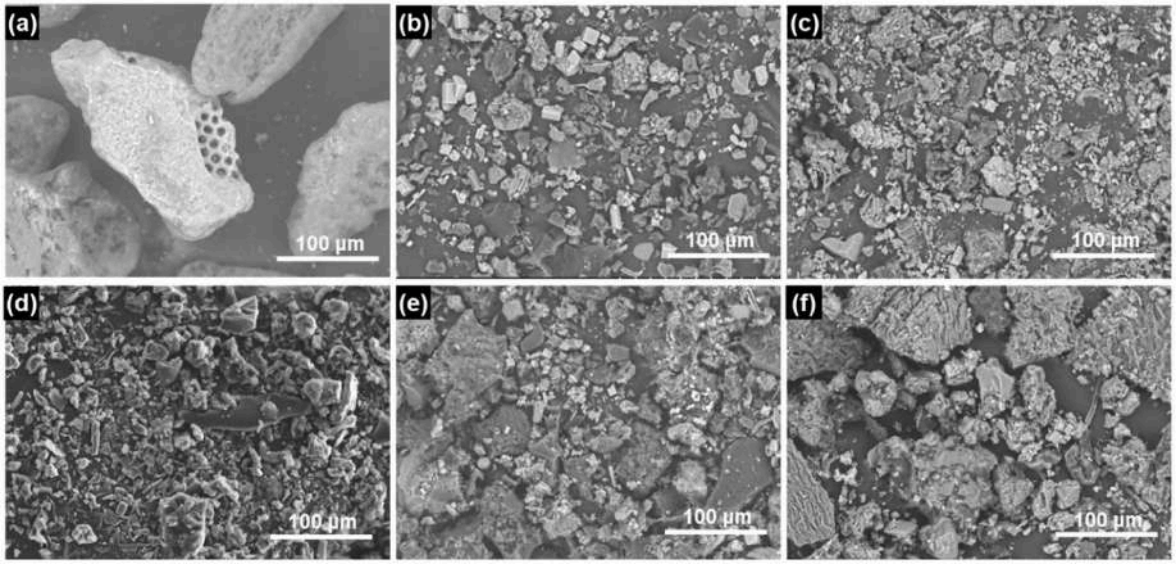

Fig. 6. SEM images of (a) *U. lactuca*, (b) biochar from 70 ULV: 30 PET, (c) biochar from 60 ULV: 40 PET, (d) biochar from 50 ULV: 50 PET, (e) biochar from 40 ULV: 60 PET, and (f) biochar from 30 ULV: 70 PET.

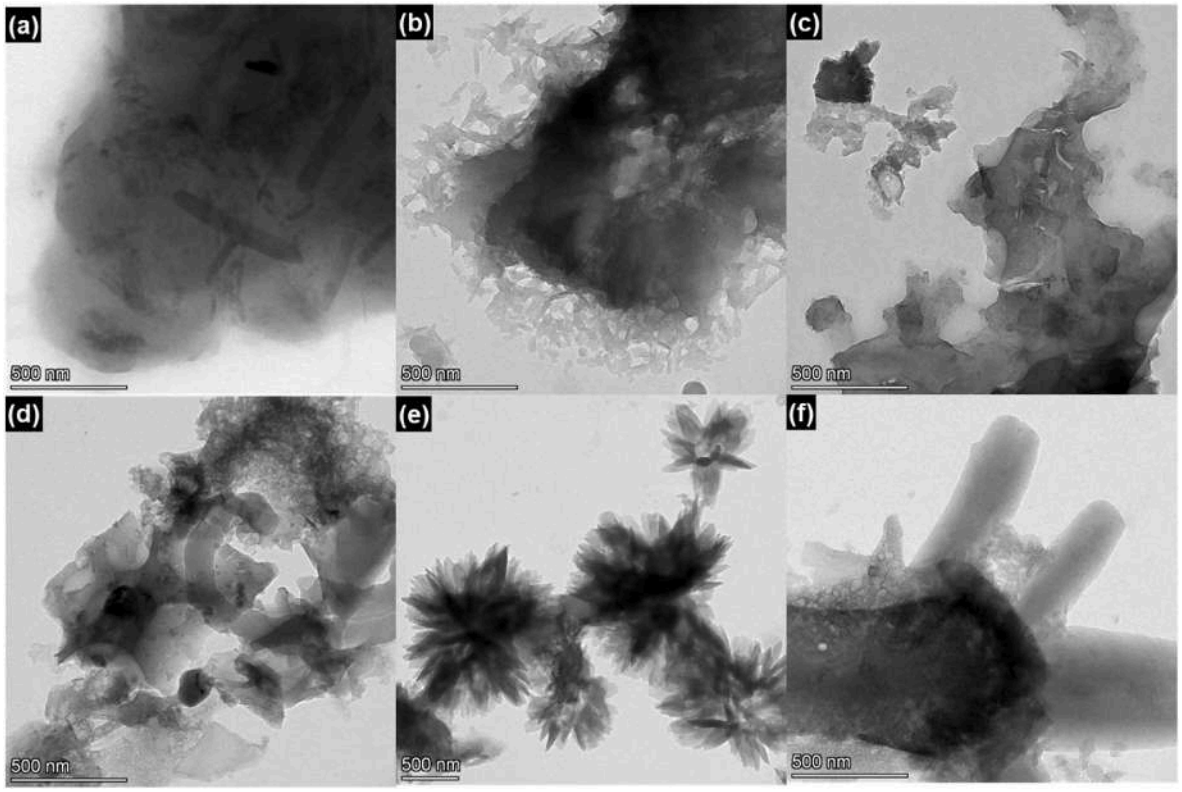

Fig. 7. HRTEM images of (a) *U. lactuca*, (b) biochar from 70 ULV: 30 PET, (c) biochar from 60 ULV: 40 PET, (d) biochar from 50 ULV: 50 PET, (e) biochar from 40 ULV: 60 PET, and (f) biochar from 30 ULV: 70 PET.

observation is that the carbon content of the biochar increases significantly, surpassing the carbon content of the pure *U. lactuca* feedstock. However, as the proportion of PET increases in the mixture, the content of C, H, N, and S in the biochar generally decreases. This trend indicates a possible interaction between the char and PET, which promotes the pyrolysis of *U. lactuca* tar and leads to the production of more volatiles [32]. In addition, the biochar samples produced from the co-pyrolysis of *U. lactuca* and PET exhibit higher HHV and LHV compared to the original feedstock, *U. lactuca*. This increase in energy content can be attributed to several factors. During the pyrolysis process, volatile compounds, such as moisture and oxygen-containing elements, are removed, resulting in a higher concentration of carbon in the biochar [28]. The carbon content, which plays a crucial role in energy generation, increases significantly in the biochar compared to the feedstock. However, as the proportion of PET in the co-pyrolysis mixture increases, the observed decrease in both HHV and LHV in the biochar can be explained by the potential interaction between PET and the biomass during the pyrolysis process. PET, a synthetic polymer, has a different

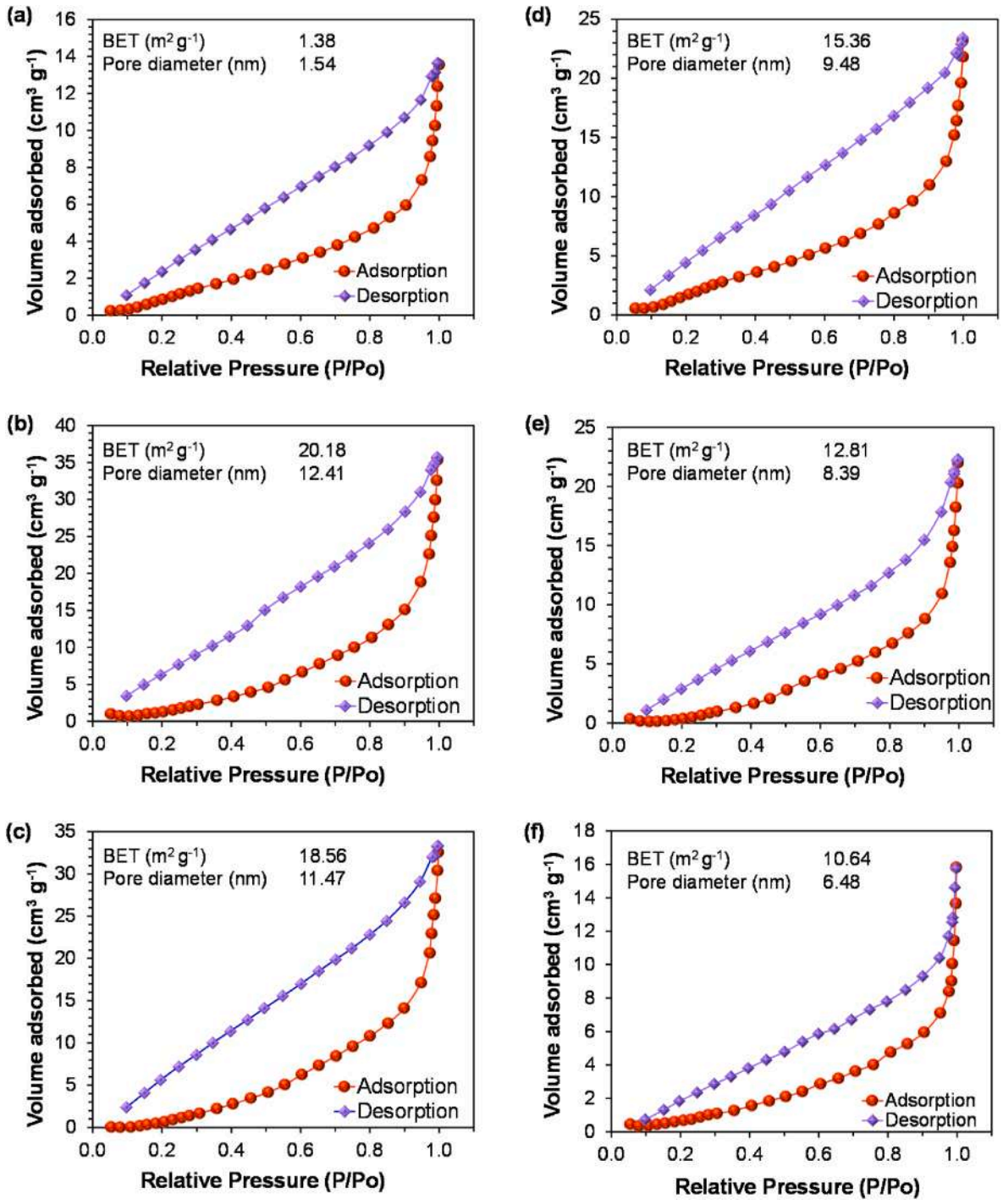

Fig. 8. BET analysis image of (a) *U. lactuca*, (b) biochar from 70 ULV: 30 PET, (c) biochar from 60 ULV: 40 PET, (d) biochar from 50 ULV: 50 PET, (e) biochar from 40 ULV: 60 PET, and (f) biochar from 30 ULV: 70 PET.

Table 2
BET surface area of *U. lactuca* and its biochar at varying feedstock ratios.

Feedstock	BET surface area [m^2 g^{-1}]	Mean pore diameter [nm]
U. lactuca	1.38	1.54
Biochar 70 ULV: 30 PET	20.18	12.41
Biochar 60 ULV: 40 PET	18.56	11.47
Biochar 50 ULV: 50 PET	15.36	9.48
Biochar 40 ULV: 60 PET	12.81	8.39
Biochar 30 ULV: 70 PET	10.64	6.48

pyrolysis behavior than biomass. When subjected to high temperatures in the presence of biomass, PET may interact with the char matrix, producing more liquid products, such as bio-oil, rather than contributing to the energy content of the solid biochar [32].

It is noteworthy that biochar has garnered significant attention for its diverse applications in agriculture, environmental management, and industrial processes. One of its most prominent uses is in carbon sequestration and soil enhancement, where biochar plays a key role in retaining carbon in soils and improving overall soil health. By increasing soil fertility and promoting better water retention, biochar supports sustainable agricultural practices while simultaneously contributing to

Table 3
Elemental analysis of biochar from co-pyrolysis of *U. lactuca* and PET.

No.	Sample	C	H	N	S	O[a]	atom O/C	atom H/C	HHV [MJ/kg]	LHV [MJ/kg]
1	*U. lactuca*	39.1	6.2	4.5	7.3	42.9	1.0972	0.1586	16.61	15.26
2	Biochar 70 ULV: 30 PET	47.3	3.9	2.9	6.4	39.5	0.8351	0.0825	17.46	16.61
3	Biochar 60 ULV: 40 PET	46.8	3.2	2.7	5.8	41.5	0.8868	0.0684	16.88	16.18
4	Biochar 50 ULV: 50 PET	46.2	2.8	2.3	5.1	43.6	0.9437	0.0606	16.47	15.86
5	Biochar 40 ULV: 60 PET	45.7	2.3	1.9	4.5	45.6	0.9978	0.0503	16.03	15.53
6	Biochar 30 ULV: 70 PET	44.8	1.8	1.4	4.2	47.8	1.0670	0.0402	15.47	15.08

[a] Calculate by difference.

efforts aimed at mitigating climate change [33]. Its ability to enrich the soil and stabilize carbon has made biochar a valuable bio-product in the fight against soil degradation and climate-related challenges.

Beyond its primary use as a soil amendment, biochar exhibits multifunctionality in various applications. Due to its porous structure, biochar is highly effective in water filtration and purification, absorbing contaminants and nutrients from water [34]. Additionally, it can be incorporated into materials such as bioplastics and concrete to improve their properties, such as enhancing durability and nutrient retention [35]. Moreover, biochar can also act as a catalyst support or carrier in chemical reactions, improving efficiency by increasing the contact between reactants and catalysts. This versatility has led to its exploration in enhancing pyrolysis reactions and converting biomass into biodiesel [36], positioning biochar as an essential material in both environmental and industrial applications.

3.5. Response surface methodology

This study utilized response surface methodology (RSM) to explore the relationships between reaction parameters and bio-oil, biochar, and gas yields during the co-pyrolysis of *U. lactuca* and PET. A total of 14 experiments were conducted following a Box-Behnken Design (BBD) to investigate the effects of temperature (A) and PET percentage (B) on the production outcomes. The quadratic regression models developed through RSM provided a robust framework for predicting yields and optimizing process conditions, demonstrating the technique's effectiveness in modeling complex chemical processes. The following equations represent the fitted quadratic models for bio-oil, biochar, and gas yields [25]:

$$\text{Bio-oil yield [\%]} = 33 + 9 \times A - 6 \times A^2 + 4 \times B^2 \quad (7)$$

$$\text{Biochar yield [\%]} = 34 - 12 \times A - 10 \times B + 9 \times A^2 - 4 \times B^2 \quad (8)$$

$$\text{Gas yield [\%]} = 45 - 10 \times A - 6 \times B - 3 \times A^2 + 2 \times B^2 \quad (9)$$

The regression equations derived from RSM revealed significant insights into how temperature and PET percentage influence the yields of bio-oil, biochar, and gas. For bio-oil, the yield was positively influenced by temperature, as indicated by the linear term, but excessive temperatures led to a decrease, as captured by the negative quadratic term. Similarly, for biochar, both temperature and PET percentage played crucial roles, with the yield decreasing at higher levels of these factors. On the other hand, the gas yield decreased with increasing temperature and PET percentage, suggesting that specific conditions favor the formation of bio-oil and biochar over gas. The accuracy of these models was validated by comparing the experimental yields with the predicted values, as illustrated in Fig. 9. The high determination coefficients (R^2 values) of 0.925 for bio-oil, 0.906 for biochar, and 0.909 for gas indicate that the models accurately predict the yields. The plot points closely follow the diagonal line, suggesting a strong correlation between the experimental and predicted data. This validates the effectiveness of the RSM in predicting the outcomes within the experimental range.

The analysis of variance (ANOVA) results provided additional validation of the models, highlighting the statistical significance of the models and their components. The ANOVA results for the quadratic models of bio-oil, biochar, and gas yields are presented in Table 4. For bio-oil, the model is highly significant ($p = 0.0008$), with temperature (A) having the most substantial effect ($p = 0.0002$). The quadratic terms for temperature (A^2) and PET percentage (B^2) are also significant, indicating that the response surface is not a simple linear function of these factors. The significant lack of fit ($p = 0.0096$) suggests that while the model is robust, there might be minor deviations in the predictions at specific experimental points. In the case of biochar, the model is significant ($p = 0.0474$), with the PET percentage playing a more prominent role compared to temperature, as seen from its lower p-value ($p = 0.0164$). The interaction and quadratic terms are less significant but still contribute to the model's accuracy. The gas yield model is also highly significant ($p = 0.0026$), with temperature having the most substantial impact. Although the PET percentage and its quadratic term (B^2) are not as significant, they still influence the gas yield, as reflected by the model.

The response surface and contour plots presented in Fig. 10 visually represented how the yields of bio-oil, biochar, and gas respond to variations in temperature and PET percentage. For bio-oil, the response surface shows a convex shape, with the maximum yield occurring at moderate temperature levels. The contour plot indicates that the yield increases with increasing PET percentage but decreases with excessively high temperatures. In contrast, the response surface for biochar is concave, with the highest biochar yield occurring at lower temperatures and PET percentages. The contour plot reveals a more complex interaction between temperature and PET percentage, where certain combinations lead to sharp decreases in yield. Meanwhile, the response surface for gas yield declines with increasing temperature and PET percentage. The contour plot highlights that high temperatures coupled with high PET percentages reduce the gas yield, suggesting that specific conditions favor the formation of bio-oil and biochar over gas.

3.6. Comparison of co-pyrolysis between U. lactuca and PET with previously reported biomass-plastic mixtures

Various biomass and plastics feedstocks have been utilized in co-pyrolysis studies to understand the synergistic effects and optimize the yield of valuable products, such as bio-oil. Common biomass feedstocks include agricultural residues from terrestrial plants (e.g., corn stalk, corn stover, and hazelnut shells) and aquatic plants (e.g., *Enteromorpha prolifera* and *Ulva lactuca*). The plastics involved in these processes include polyethylene (PE), polyvinyl chloride (PVC), polystyrene (PS), polyethylene terephthalate (PET), high-density polyethylene (HDPE), and low-density polyethylene (LDPE).

Table 5 shows the bio-oil yields obtained from co-pyrolysis of various biomasses and plastics. The *U. lactuca*-PET mixture resulted in a relatively higher bio-oil yield than mixtures such as *Enteromorpha prolifera*-HDPE (27.2 %) and elephant grass-LDPE (27.30 %). These differences could be attributed to the type of plastic and biomass used, as well as the pyrolysis conditions, particularly the temperature and feedstock ratio [37]. The yield of 37.91 % was moderate when compared to the 41.71 % yield obtained from the co-pyrolysis of *Enteromorpha clathrate* and PVC, which was performed at a higher temperature (550 °C) and different biomass-to-plastic ratio (4:1). The increased yield of *Enteromorpha clathrate*-PVC could be due to the higher temperature, which may enhance

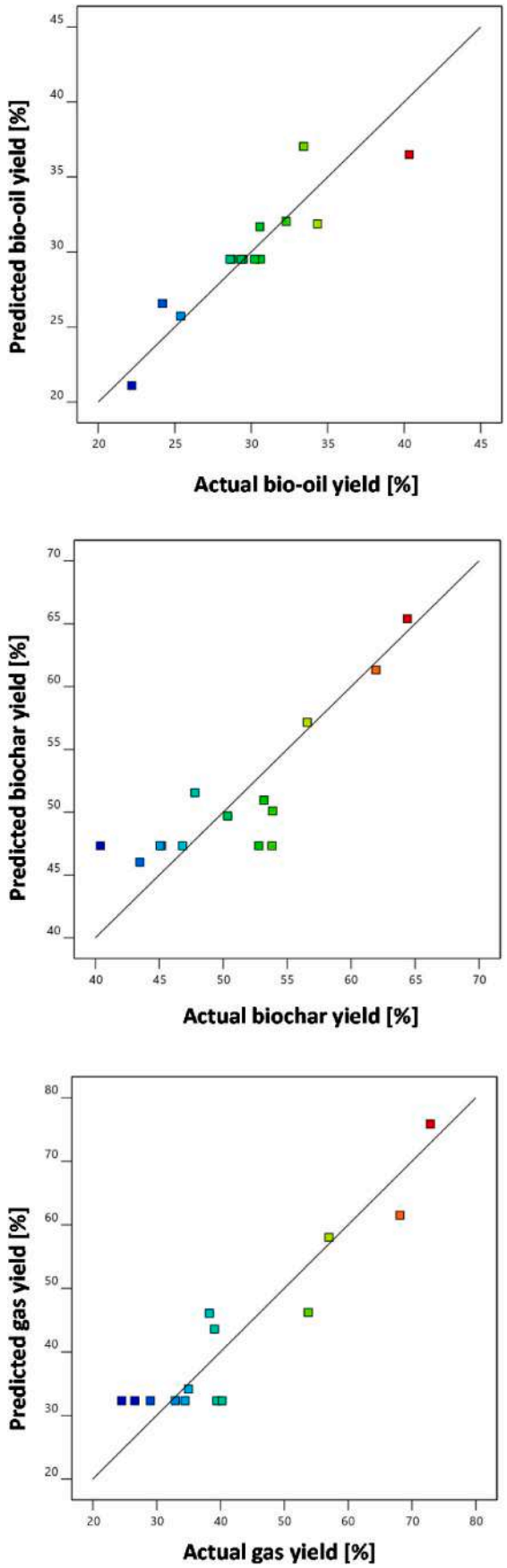

Fig. 9. Actual versus predicted plots for bio-oil, biochar, and gas yields.

the thermal degradation of biomass and plastic, leading to a more efficient conversion to bio-oil [28]. This indicates that not only the type of biomass and plastic but also the pyrolysis temperature and feedstock ratio play critical roles in determining the bio-oil yield.

3.7. Reaction kinetics

The reaction rate constant plays a crucial role in comprehending how solid biomass behaves during thermochemical processes. To determine the reaction rate constant for solid degradation in pyrolysis, one can use the formula for a first-order reaction. The model representing solid degradation in pyrolysis can be formulated based on our previously published study as follows:

$$X_{ULV\ and\ PET} \rightarrow \nu X_{bio-oil} + (1-\nu)X_{solid} \tag{10}$$

In this context, $X_{ULV\ \text{and}\ \text{PET}}$ refer to the initial ratios of *U. lactuca* and PET feedstocks. Variable ν represents the amount of solids converted into bio-oil. $X_{bio\text{-}oil}$ and X_{solid} are defined as the fractions of bio-oil generated and the remaining solid material, respectively. Assuming a first-order kinetic process, the differential rate expression for the feedstock conversion at a given time (t) can be established using the following formula:

$$\frac{d\,[X_{ULV\ and\ PET}]}{d_t} = -k[X_{ULV\ and\ PET}] \tag{11}$$

Considering the principles of mass balance, the equation can be expressed as follows:

$$[X_{ULV\ and\ PET}] + [X_{liquid}] + [X_{solid}] = \text{constant} = [X_{ULV\ and\ PET}]_i + [X_{liquid}]_i + [X_{solid}]_i = [X_{ULV\ and\ PET}]_t \tag{12}$$

In this notation, 'i' represents the initial value, while 't' denotes the total amount of *U. lactuca* and PET present during pyrolysis. Likewise, the amounts of $X_{ULV\ \text{and}\ \text{PET}}$ can be measured and described as follows:

$$[X_{ULV\ and\ PET}] = \frac{1-\nu}{\nu}[X_{liquid}] \tag{13}$$

By substituting Eq. (13) into Eq. (12), we can express the mass balance equation as follows:

$$\begin{aligned}[X_{ULV\ and\ PET}] &= [X_{ULV\ and\ PET}]_t - [X_{liquid}] - [X_{solid}] = [X_{ULV\ and\ PET}]_t - [X_{liquid}] \\ &\quad - \frac{1-\nu}{\nu}[X_{liquid}] = [X_{ULV\ and\ PET}]_t - \left(1+\frac{1-\nu}{\nu}\right)[X_{liquid}] \\ &= [X_{ULV\ and\ PET}]_t - \frac{1}{\nu}[X_{liquid}]\end{aligned} \tag{14}$$

Following this, by substituting Eq. (11) for Eq. (14), we can determine the rate of change, which is presented as follows:

$$\frac{d}{dt}\left([X_{ULV\ and\ PET}]_t - \frac{1}{\nu}[X_{liquid}]\right) = -k\left([X_{ULV\ and\ PET}]_t - \frac{1}{\nu}[X_{liquid}]\right) \tag{15}$$

$$\frac{d}{dt}\left([X_{liquid}]\right) = \nu k\left([X_{ULV\ and\ PET}]_t - \frac{1}{\nu}[X_{liquid}]\right) \tag{16}$$

On the other hand, the yield of the liquid product can be expressed as follows:

$$Y_{liquid} = \frac{[X_{liquid}]}{[X_{ULV\ and\ PET}]_t} \tag{17}$$

As a result, Eq. (16) can be presented as:

$$\frac{d}{dt}Y_{liquid} = \nu k - kY_{liquid} \tag{18}$$

Equation (18) can be reformulated as follows:

Table 4
One-way analysis of variance (ANOVA) for the fitted polynomial quadratic model of bio-oil, biochar, and gas yields.

Source	Sum of square	df	Mean square	F-value	p-value	Note
(a) bio-oil						
Model	1.83	5	0.3666	17.34	0.0008	significant
A-Temperature	1.11	1	1.11	52.41	0.0002	
B-PET Percentage	0.1453	1	0.1453	6.87	0.0343	
AB	0.035	1	0.035	1.66	0.239	
A^2	0.1806	1	0.1806	8.54	0.0223	
B^2	0.3239	1	0.3239	15.32	0.0058	
Residual	0.148	7	0.0211			
Lack of Fit	0.1373	3	0.0458	17.07	0.0096	significant
Pure Error	0.0107	4	0.0027			
Cor Total	2.17	13				
(b) biochar						
Model	2.1	5	0.42	4.06	0.0474	significant
A-Temperature	0.0078	1	0.0078	0.0752	0.7919	
B-PET Percentage	1.02	1	1.02	9.86	0.0164	
AB	0.1116	1	0.1116	1.08	0.3335	
A^2	0.0853	1	0.0853	0.8251	0.3939	
B^2	0.9136	1	0.9136	8.84	0.0207	
Residual	0.7237	7	0.1034			
Lack of Fit	0.1164	3	0.0388	0.2555	0.8543	not significant
Pure Error	0.6074	4	0.1518			
Cor Total	2.99	13				
(c) gas						
Model	13.2	5	2.64	11.89	0.0026	significant
A-Temperature	4.46	1	4.46	20.06	0.0029	
B-PET Percentage	0.9007	1	0.9007	4.05	0.0839	
AB	0.1986	1	0.1986	0.8937	0.376	
A^2	7.22	1	7.22	32.48	0.0007	
B^2	0.7397	1	0.7397	3.33	0.1108	
Residual	1.56	7	0.2222			
Lack of Fit	0.5172	3	0.1724	0.6644	0.6162	not significant
Pure Error	1.04	4	0.2595			
Cor Total	15.91	13				

$$\frac{dY_{liquid}}{vt - kY_{liquid}} = dt \tag{19}$$

$$ln(v - Y_{liquid}) = -kt + C \tag{20}$$

$$Y_{liquid} = v - A\ exp(-kt)) \tag{21}$$

The rate constant can be determined using the Arrhenius equation, which is described as follows:

$$k = A\ exp\left(\frac{E_a}{RT}\right) \tag{22}$$

Here, 'T' represents the temperature, 'Ea' indicates the activation energy, 'A' signifies the frequency factor, and 'R' is the universal gas constant. After integrating the Arrhenius expression into Eq. (21), the updated formula is expressed as:

$$Y_{liquid} = v - (v - Y_{liquid.i})exp\left(-A\ exp\left(\frac{E_a}{RT}\right)t\right) \tag{23}$$

The reaction rate constant and the percentage of solid material transformed into the liquid phase were calculated using the least-squares error (LSE) approach. Fig. 11 demonstrates the correlation between the experimental data and theoretical predictions, highlighting the influence of temperature on bio-oil yield. A strong agreement was observed between the experimental results and the theoretical model.

This was further supported by the parity diagrams, which demonstrated a high coefficient of determination (R^2) of 0.9995, as shown in Fig. 12. Fig. 13 presents the Arrhenius plot that outlines the decomposition rate of co-pyrolysis of *U. lactuca* and PET. From this graph, both the activation energy and the frequency factor were derived. It is worth noting that the activation energy was calculated under optimal conditions (500 °C and a feedstock composition of 40 % *U. lactuca* and 60 % PET). The frequency factor for co-pyrolysis of *U. lactuca* and PET is estimated to be around 0.351 s^{-1}. Additionally, the calculated activation energy for this process is approximately 43.35 kJ mol^{-1}. This value is significantly lower compared to previous studies. For example, Burra et al. (2018) [47] reported an activation energy of 50 kJ/mol for the co-pyrolysis of pinewood and polycarbonate, while Varma et al. (2021) [48] documented an even higher range of 96.44–109.73 kJ/mol for the co-pyrolysis of pine needles and styrofoam.

The lower activation energy in this study could be attributed to the specific blend of feedstocks used, which consists of 40 % *U. lactuca* and 60 % PET. This blend differs substantially from the biomass and polymer combinations in other studies. *U. lactuca* has a less complex and more thermally reactive chemical structure than pinewood, pine needles, and the polymers used in those studies. For example, marine algae like *U. lactuca* contain simpler polysaccharides such as ulvan, which break down more easily than the lignin and cellulose structures found in woody biomass. As a result, less energy is required to initiate decomposition in the co-pyrolysis process.

4. Conclusion

This study advances sustainable energy production and marine pollution mitigation by examining *U. lactuca* macroalgae and PET co-pyrolysis. The optimal conditions of 500 °C and 40 % *U. lactuca* to 60 % PET ratio produced the highest bio-oil yield of 37.91 %. This notably enhanced the quality of bio-oil by enhancing hydrocarbon content and suppressing undesirable compounds. The produced biochar improved surface area and porosity, although these values decreased with increasing PET ratios. This makes biochar a valuable by-product for applications such as soil amendment and wastewater treatment, contributing to environmental sustainability. The reaction kinetics analysis revealed that the co-pyrolysis process follows a first-order reaction model, with the reaction rate constant and activation energy calculated to be 43.35 kJ/mol under optimal conditions. Future research should focus on optimizing parameters, such as reaction time and

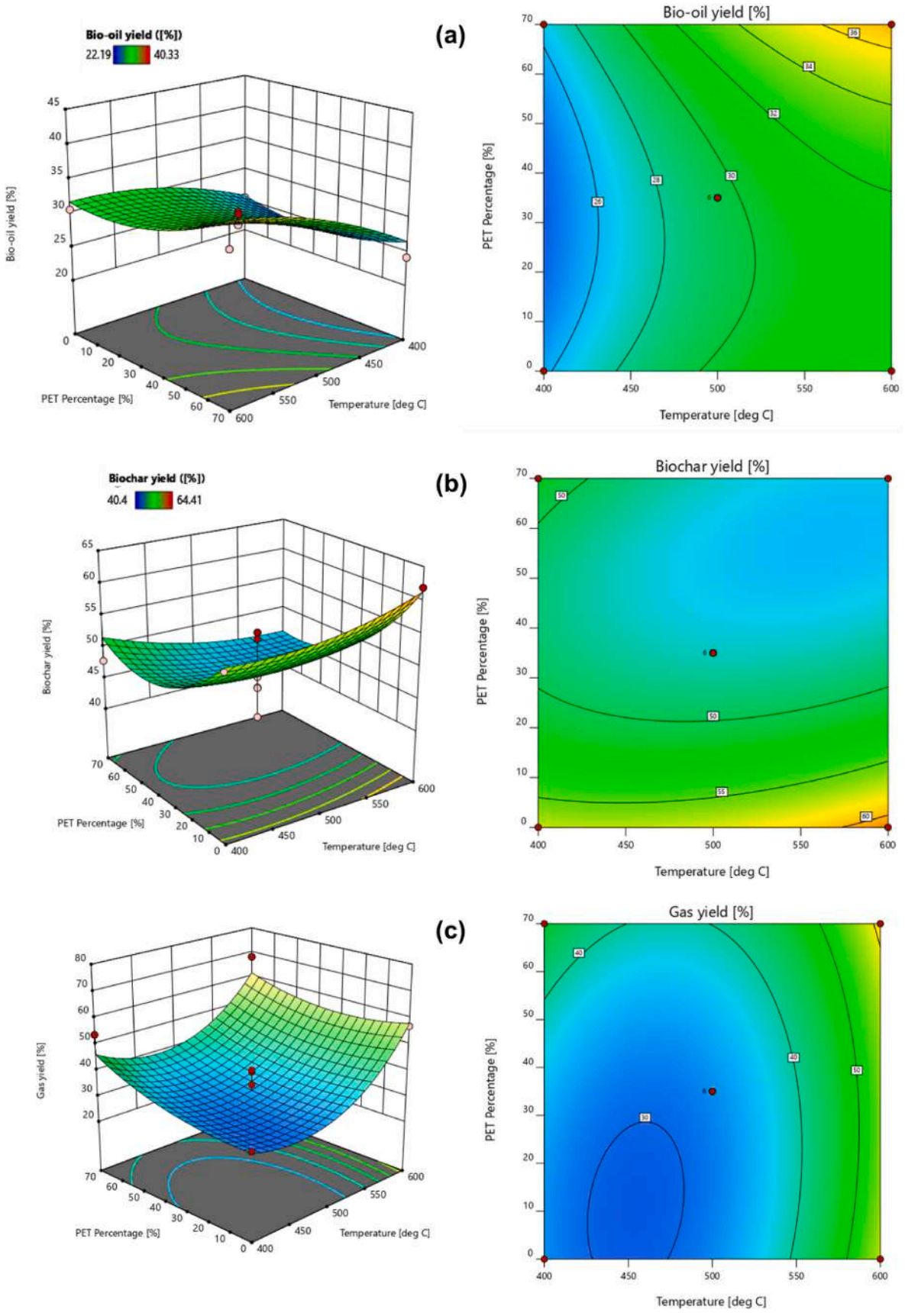

Fig. 10. Response surface and contour plots of %yield for (a) bio-oil, (b) biochar, and (c) gas.

Table 5
Bio-oil yields obtained from co-pyrolysis of various biomasses and plastics.

Biomass type	Plastic type	Temperature [°C]	Biomass-to-plastic ratio	Bio-oil yield [%]	Reference
U. lactuca	PET	500	2:3	37.91	This study
Enteromorpha clathrate	PVC	550	4:1	41.71	Cao et al. [38]
Enteromorpha prolifera	HDPE	500	4:1	27.2	Uzoejinwa et al. [39]
Elephant grass	LDPE	382	35:1	27.30	Adeniyi et al. [40]
Cotton stalk	PVC	800	1:1	21.21	Çepeliogullar and Putun [41]
Hazelnut shells	PVC	500	1:1	28.01	Çepeliogullar and Putun [42]
Pine cone	PS	500	1:1	21.50	Brebu et al. [43]
Poplar wood	PS	750	9:1	19.90	Ephraim et al. [44]
Corn stalk	PE	600	1:1	20.00	Fan et al. [45]
Corn stover	HDPE	550	2:1	17.10	Lin et al. [46]

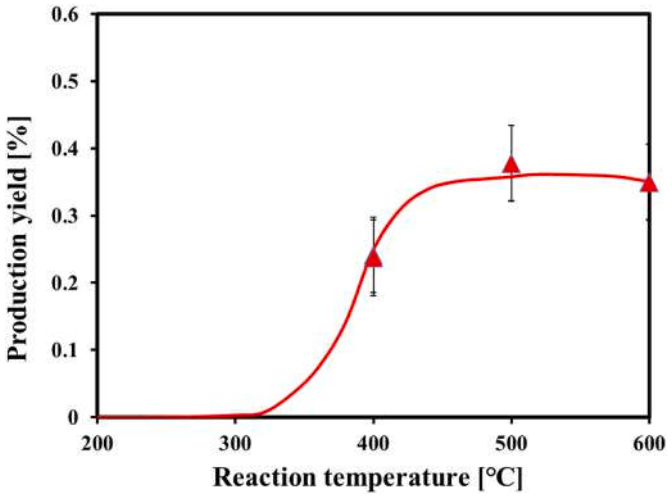

Fig. 11. The curve-fitting analysis demonstrating the bio-oil yield at different temperatures observed during the co-pyrolysis process of *U. lactuca* and PET.

feedstock particle size, as well as exploring larger-scale and continuous-flow processes to assess commercial viability. Implementing this co-pyrolysis approach globally could effectively manage plastic waste and marine biomass, thereby addressing both energy demands and environmental preservation.

CRediT authorship contribution statement

Obie Farobie: Writing – review & editing, Writing – original draft, Resources, Project administration, Funding acquisition, Formal analysis, Conceptualization. **Apip Amrullah:** Resources, Investigation, Formal analysis. **Widya Fatriasari:** Writing – review & editing, Resources, Formal analysis. **Asep Bayu Dani Nandiyanto:** Resources, Methodology. **Lusi Ernawati:** Writing – review & editing, Formal analysis. **Surachai Karnjanakom:** Writing – review & editing, Methodology. **Seng Hua Lee:** Writing – review & editing, Conceptualization. **Rangabhashiyam Selvasembian:** Writing – review & editing, Conceptualization. **Nur Izyan Wan Azelee:** Writing – review & editing, Conceptualization. **Muhammad Aziz:** Writing – review & editing, Conceptualization.

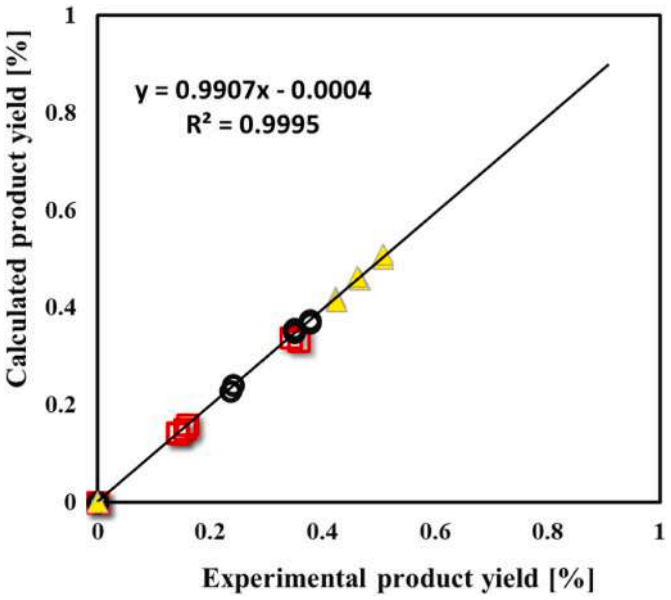

Fig. 12. Plots of parity showcasing a comparison between bio-oil yields derived from experimental measurements and those predicted through calculations.

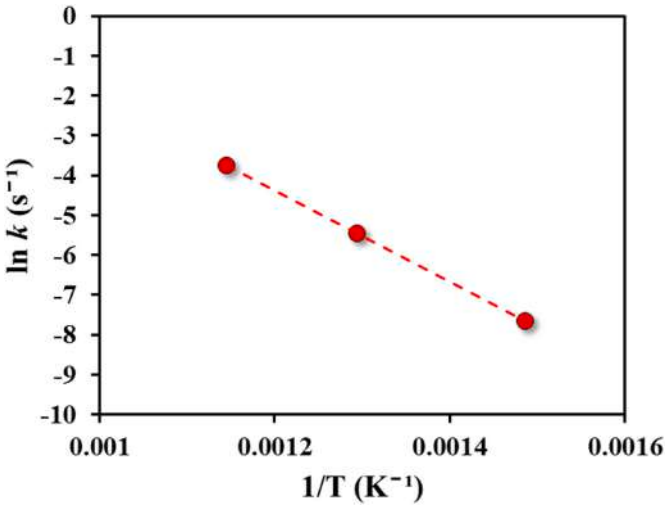

Fig. 13. Arrhenius graphs for the thermal decomposition during the co-pyrolysis of *U. lactuca* and PET.

Declaration of competing interest

The authors declare that they have no known competing financial interests or personal relationships that could have appeared to influence the work reported in this paper.

Acknowledgment

The authors express gratitude for the support provided by the Bank Indonesia Institute through the Research Grant of Bank Indonesia (Grant No. 25/22/PKS/BINS/2023). This study also received partial support from the Equity Program through an international research collaboration (574/IT3.D10/PT.01.03/P/B/2023).

Data availability

Data will be made available on request.

References

[1] M.H. Ali, M.N.A. Moral, Pyrolytic fuel extraction from tire and tube: analysis of parameters on product yield, Case Stud. Chem. Environ. Eng. 6 (2022) 100273, https://doi.org/10.1016/j.cscee.2022.100273.

[2] R.A. Aljeradat, S.H. Aljbour, N.A. Jarrah, Performance of chemically modified Tripoli in catalytic pyrolysis of date kernels, Case Stud. Chem. Environ. Eng. 7 (2023) 100319, https://doi.org/10.1016/j.cscee.2023.100319.

[3] B.V. Ayodele, M.A. Alsaffar, S.I. Mustapa, An overview of integration opportunities for sustainable bioethanol production from first- and second-generation sugar-based feedstocks, J. Clean. Prod. 245 (2020) 118857, https://doi.org/10.1016/j.jclepro.2019.118857.

[4] A.H. Hirani, N. Javed, M. Asif, S.K. Basu, A. Kumar, A review on first- and second-generation biofuel productions, Biofuels Greenh. Gas Mitig. Glob. Warm. Next Gener. Biofuels Role Biotechnol. (2018) 141–154, https://doi.org/10.1007/978-81-322-3763-1_8.

[5] O. Farobie, N. Syaftika, I. Masfuri, T.P. Rini, D.P.A. Lanank Es, A. Bayu, A. Amrullah, E. Hartulistiyoso, N.R. Moheimani, S. Karnjanakom, Y. Matsumura, Green algae to green fuels: syngas and hydrochar production from Ulva lactuca via sub-critical water gasification, Algal Res. 67 (2022) 102834, https://doi.org/10.1016/j.algal.2022.102834.

[6] A. Bruhn, J. Dahl, H.B. Nielsen, L. Nikolaisen, M.B. Rasmussen, S. Markager, B. Olesen, C. Arias, P.D. Jensen, Bioenergy potential of Ulva lactuca: biomass yield, methane production and combustion, Bioresour. Technol. 102 (2011) 2595–2604, https://doi.org/10.1016/j.biortech.2010.10.010.

[7] O. Babich, S. Ivanova, P. Michaud, E. Budenkova, E. Kashirskikh, V. Anokhova, S. Sukhikh, Fermentation of micro- and macroalgae as a way to produce value-added products, Biotechnol. Reports 41 (2024) e00827, https://doi.org/10.1016/j.btre.2023.e00827.

[8] M. Chen, Y. Chen, Q. Zhang, Assessing global carbon sequestration and bioenergy potential from microalgae cultivation on marginal lands leveraging machine learning, Sci. Total Environ. 948 (2024) 174462, https://doi.org/10.1016/j.scitotenv.2024.174462.

[9] E. Allen, J. Browne, S. Hynes, J.D. Murphy, The potential of algae blooms to produce renewable gaseous fuel, Waste Manag. 33 (2013) 2425–2433, https://doi.org/10.1016/j.wasman.2013.06.017.

[10] A. Amrullah, O. Farobie, R. Widyanto, Pyrolysis of purun tikus (Eleocharis dulcis): product distributions and reaction kinetics, Bioresour. Technol. Rep. 13 (2021) 100642, https://doi.org/10.1016/j.biteb.2021.100642.

[11] K.W. Kuttin, H. Yu, M. Yang, L. Ding, X. Chen, G. Yu, F. Wang, Experimental and numerical modeling of carbonized biomass gasification: a critical review, Green Carbon 2 (2024) 176–196, https://doi.org/10.1016/j.greenca.2024.04.003.

[12] M. Usman, S. Cheng, S. Boonyubol, J.S. Cross, From biomass to biocrude: innovations in hydrothermal liquefaction and upgrading, Energy Convers. Manag. 302 (2024) 118093, https://doi.org/10.1016/j.enconman.2024.118093.

[13] A.B. Ross, J.M. Jones, M.L. Kubacki, T. Bridgeman, Classification of macroalgae as fuel and its thermochemical behaviour, Bioresour. Technol. 99 (2008) 6494–6504, https://doi.org/10.1016/j.biortech.2007.11.036.

[14] O. Farobie, A. Amrullah, A. Bayu, N. Syaftika, L.A. Anis, E. Hartulistiyoso, In-depth study of bio-oil and biochar production from macroalgae Sargassum sp. via slow pyrolysis, RSC Adv. 12 (2022) 9567–9578, https://doi.org/10.1039/d2ra00702a.

[15] B. Cao, Y. Sun, J. Guo, S. Wang, J. Yuan, S. Esakkimuthu, B. Bernard Uzoejinwa, C. Yuan, A.E.F. Abomohra, L. Qian, L. Liu, B. Li, Z. He, Q. Wang, Synergistic effects of co-pyrolysis of macroalgae and polyvinyl chloride on bio-oil/bio-char properties and transferring regularity of chlorine, Fuel 246 (2019) 319–329, https://doi.org/10.1016/j.fuel.2019.02.037.

[16] M.H.M. Ahmed, N. Batalha, H.M.D. Mahmudul, G. Perkins, M. Konarova, A review on advanced catalytic co-pyrolysis of biomass and hydrogen-rich feedstock: insights into synergistic effect, catalyst development and reaction mechanism, Bioresour. Technol. 310 (2020) 123457, https://doi.org/10.1016/j.biortech.2020.123457.

[17] J. Yang, J. Rizkiana, W.B. Widayatno, S. Karnjanakom, M. Kaewpanha, X. Hao, A. Abudula, G. Guan, Fast co-pyrolysis of low density polyethylene and biomass residue for oil production, Energy Convers. Manag. 120 (2016) 422–429, https://doi.org/10.1016/j.enconman.2016.05.008.

[18] B. Cao, Y. Sun, J. Guo, S. Wang, J. Yuan, S. Esakkimuthu, B. Bernard Uzoejinwa, C. Yuan, A.E.F. Abomohra, L. Qian, L. Liu, B. Li, Z. He, Q. Wang, Synergistic effects of co-pyrolysis of macroalgae and polyvinyl chloride on bio-oil/bio-char properties and transferring regularity of chlorine, Fuel 246 (2019) 319–329, https://doi.org/10.1016/j.fuel.2019.02.037.

[19] H.W. Lee, S.J. Choi, S.H. Park, J.K. Jeon, S.C. Jung, S.C. Kim, Y.K. Park, Pyrolysis and co-pyrolysis of Laminaria japonica and polypropylene over mesoporous Al-SBA-15 catalyst, Nanoscale Res. Lett. 9 (2014) 1–8, https://doi.org/10.1186/1556-276X-9-376.

[20] J.A. Oyebanji, P.O. Okekunle, O.A. Lasode, S.O. Oyedepo, Chemical composition of bio-oils produced by fast pyrolysis of two energy biomass, Biofuels 9 (2018) 479–487, https://doi.org/10.1080/17597269.2017.1284473.

[21] E. Hartulistiyoso, O. Farobie, L.A. Anis, N. Syaftika, A. Bayu, A. Amrullah, N. R. Moheimani, S. Karnjanakom, Y. Matsumura, Co-production of hydrochar and bioactive compounds from Ulva lactuca via a hydrothermal process, Carbon Resour. Convers. 7 (2024), https://doi.org/10.1016/j.crcon.2023.05.002.

[22] S. Xu, B. Cao, B.B. Uzoejinwa, E.A. Odey, S. Wang, H. Shang, C. Li, Y. Hu, Q. Wang, J.N. Nwakaire, Synergistic effects of catalytic co-pyrolysis of macroalgae with waste plastics, Process Saf. Environ. Protect. 137 (2020) 34–48, https://doi.org/10.1016/j.psep.2020.02.001.

[23] Z. Alhulaybi, I. Dubdub, Comprehensive kinetic study of PET pyrolysis using TGA, Polymers 15 (2023), https://doi.org/10.3390/polym15143010.

[24] A.E.F. Abomohra, H.M.A. Sheikh, A.H. El-Naggar, Q. Wang, Microwave vacuum co-pyrolysis of waste plastic and seaweeds for enhanced crude bio-oil recovery: experimental and feasibility study towards industrialization, Renew. Sustain. Energy Rev. 149 (2021) 111335, https://doi.org/10.1016/j.rser.2021.111335.

[25] A. Amrullah, O. Farobie, H. Irawansyah, M. Lutfi, L. Noviani Haty, Synergistic enhancement of bio-oil production, quality, and optimization from co-pyrolysis purun tikus (Eleocharis dulcis) and plastic waste using response surface methodology, Process Saf. Environ. Protect. 187 (2024) 471–482, https://doi.org/10.1016/j.psep.2024.04.079.

[26] L. Fan, P. Chen, Y. Zhang, S. Liu, Y. Liu, Y. Wang, L. Dai, R. Ruan, Fast microwave-assisted catalytic co-pyrolysis of lignin and low-density polyethylene with HZSM-5 and MgO for improved bio-oil yield and quality, Bioresour. Technol. 225 (2017) 199–205, https://doi.org/10.1016/j.biortech.2016.11.072.

[27] A. Selvarajoo, D. Oochit, Effect of pyrolysis temperature on product yields of palm fibre and its biochar characteristics, Mater. Sci. Energy Technol. 3 (2020) 575–583, https://doi.org/10.1016/j.mset.2020.06.003.

[28] A. Iaccarino, R. Gautam, S.M. Sarathy, Bio-oil and biochar production from halophyte biomass: effects of pre-treatment and temperature on Salicornia bigelovii pyrolysis, Sustain. Energy Fuels 5 (2021) 2234–2248, https://doi.org/10.1039/d0se01664k.

[29] A. Aboulkas, H. Hammani, M. El Achaby, E. Bilal, A. Barakat, K. El harfi, Valorization of algal waste via pyrolysis in a fixed-bed reactor: production and characterization of bio-oil and bio-char, Bioresour. Technol. 243 (2017) 400–408, https://doi.org/10.1016/j.biortech.2017.06.098.

[30] S. Iannello, A. Sebastiani, M. Errigo, M. Materazzi, The behaviour of plastic particles during pyrolysis in bubbling fluidized bed reactors: incipient agglomeration and axial segregation, Powder Technol. 441 (2024) 119846, https://doi.org/10.1016/j.powtec.2024.119846.

[31] A.I. Osman, C. Farrell, A.H. Al-Muhtaseb, J. Harrison, D.W. Rooney, The production and application of carbon nanomaterials from high alkali silicate herbaceous biomass, Sci. Rep. 10 (2020) 1–13, https://doi.org/10.1038/s41598-020-59481-7.

[32] Z. Tang, W. Chen, Y. Chen, H. Yang, H. Chen, Co-pyrolysis of microalgae and plastic: characteristics and interaction effects, Bioresour. Technol. 274 (2019) 145–152, https://doi.org/10.1016/j.biortech.2018.11.083.

[33] M. Afshar, S. Mofatteh, Biochar for a sustainable future: environmentally friendly production and diverse applications, Results Eng 23 (2024) 102433, https://doi.org/10.1016/j.rineng.2024.102433.

[34] H.M.M. Abbas, U. Rais, M.M. Altaf, F. Rasul, A. Shah, A. Tahir, M. Nafees-Ur-Rehman, M. Shaukat, H. Sultan, R. Zou, M.N. Khan, L. Nie, Microbial-inoculated biochar for remediation of salt and heavy metal contaminated soils, Sci. Total Environ. 954 (2024) 176104, https://doi.org/10.1016/j.scitotenv.2024.176104.

[35] S.S. Senadheera, S. Gupta, H.W. Kua, D. Hou, S. Kim, D.C.W. Tsang, Y.S. Ok, Application of biochar in concrete – a review, Cem. Concr. Compos. 143 (2023) 105204, https://doi.org/10.1016/j.cemconcomp.2023.105204.

[36] O. Farobie, N.F. Santosa, W. Fatriasari, A. Karimah, A. Amrullah, S.H. Suseno, A.B. D. Nandiyanto, E. Hartulistiyoso, Harnessing macroalgae Sargassum plagiophyllum-derived heterogeneous catalyst for biodiesel production, Bioresour. Technol. Rep. 25 (2024) 101768, https://doi.org/10.1016/j.biteb.2024.101768.

[37] A.G. Adeniyi, K.O. Iwuozor, E.C. Emenike, O.J. Ajala, S. Ogunniyi, K.B. Muritala, Thermochemical co-conversion of biomass-plastic waste to biochar: a review, Green Chem. Eng. 5 (2024) 31–49, https://doi.org/10.1016/j.gce.2023.03.002.

[38] B. Cao, Y. Sun, J. Guo, S. Wang, J. Yuan, S. Esakkimuthu, B. Bernard Uzoejinwa, C. Yuan, A.E.F. Abomohra, L. Qian, L. Liu, B. Li, Z. He, Q. Wang, Synergistic effects of co-pyrolysis of macroalgae and polyvinyl chloride on bio-oil/bio-char properties and transferring regularity of chlorine, Fuel 246 (2019) 319–329, https://doi.org/10.1016/j.fuel.2019.02.037.

[39] B.B. Uzoejinwa, X. He, S. Wang, A.E.F. Abomohra, Y. Hu, Z. He, Q. Wang, Co-pyrolysis of seaweeds with waste plastics: modeling and simulation of effects of co-pyrolysis parameters on yields, and optimization studies for maximum yield of enhanced biofuels, Energy Sources, Part A Recover. Util. Environ. Eff. 42 (2020) 954–978, https://doi.org/10.1080/15567036.2019.1602209.

[40] A.G. Adeniyi, J.O. Ighalo, D. V Onifade, A.O. Popoola, Production of hybrid biochar by retort-heating of elephant grass (pennisetum purpureum) and low density polyethylene (LDPE) for waste management and product development, J. Mater. Environ. Sci. 2020 (2020) 1940–1952.

[41] Ö. Çepelioğullar, A.E. Pütün, Thermal and kinetic behaviors of biomass and plastic wastes in co-pyrolysis, Energy Convers. Manag. 75 (2013) 263–270, https://doi.org/10.1016/j.enconman.2013.06.036.

[42] Ö. Çepelioǂullar, A.E. Pütün, Products characterization study of a slow pyrolysis of biomass-plastic mixtures in a fixed-bed reactor, J. Anal. Appl. Pyrolysis 110 (2014) 363–374, https://doi.org/10.1016/j.jaap.2014.10.002.

[43] M. Brebu, S. Ucar, C. Vasile, J. Yanik, Co-pyrolysis of pine cone with synthetic polymers, Fuel 89 (2010) 1911–1918, https://doi.org/10.1016/j.fuel.2010.01.029.

[44] A. Ephraim, D.P. Minh, D. Lebonnois, C. Peregrina, P. Sharrock, A. Nzihou, A. Ephraim, D.P. Minh, D. Lebonnois, C. Peregrina, P. Sharrock, Co-pyrolysis of Wood and Plastics to Cite This Version : HAL Id : Hal-01802140, 2018.

[45] S. Fan, Y. Sun, T. Yang, Y. Chen, B. Yan, R. Li, G. Chen, Biochar derived from corn stalk and polyethylene co-pyrolysis: characterization and Pb(ii) removal potential, RSC Adv. 10 (2020) 6362–6376, https://doi.org/10.1039/c9ra09487c.

[46] X. Lin, D. Zhang, X. Ren, Q. Zhang, H. Cai, W. Yi, H. Lei, Catalytic co-pyrolysis of waste corn stover and high-density polyethylene for hydrocarbon production: the coupling effect of potassium and HZSM-5 zeolite, J. Anal. Appl. Pyrolysis 150 (2020) 104895, https://doi.org/10.1016/j.jaap.2020.104895.

[47] K.G. Burra, A.K. Gupta, Kinetics of synergistic effects in co-pyrolysis of biomass with plastic wastes, Appl. Energy 220 (2018) 408–418, https://doi.org/10.1016/j.apenergy.2018.03.117.

[48] A.K. Varma, N. Lal, A.K. Rathore, R. Katiyar, L.S. Thakur, R. Shankar, P. Mondal, Thermal, kinetic and thermodynamic study for co-pyrolysis of pine needles and styrofoam using thermogravimetric analysis, Energy 218 (2021) 119404, https://doi.org/10.1016/j.energy.2020.119404.